Metalens for intersatellite free-space optical communications

Badas Aldecocea, M.; Algera, J.; Bouwmeester, J.; Piron, P.; Loicq, Jérôme

DOI
10.1117/12.3075404

Publication date
2025

Document Version
Final published version

Published in
International Conference on Space Optics — ICSO 2024

International Conference on Space Optics—ICSO 2024
Antibes Juan-les-Pins, France
21-25 October 2024

Edited by Philippe Kubik, Frédéric Bernard, Kyriaki Minoglou and Nikos Karafolas

Metalens for intersatellite free space optical communications

International Conference on Space Optics — ICSO 2024, edited by Frédéric Bernard, Nikos Karafolas, Philippe Kubik, Kyriaki Minoglou, Proc. of SPIE Vol. 13699, 1369913 · © 2025 ESA and CNES · 0277-786X · doi: 10.1117/12.3075404

Metalens for intersatellite free space optical communications

Mario Badás Aldecocea[a], Johannes Algera[a], Jasper Bouwmeester[a], Pierre Piron[a], and Jérôme Loicq[a,b]

[a]Department of Space Engineering, Delft University of Technology, Kluyverweg 1, 2629 HS Delft, Netherlands
[b]STAR Institute, University of Liège, Avenue du Pré Aily, 4031 Liège, Belgium

ABSTRACT

Metamaterials and metasurfaces hold significant promise for space applications due to their compactness and lightweight characteristics. These devices use nanostructures embedded in their flat surfaces to manipulate the electromagnetic field for various purposes. Among their potential applications, metalenses stand out for their prospective role in the next generation of optical instruments deployed in space. Specifically, they offer considerable advantages for free space optical and quantum communications terminals. In intersatellite free space optical communication links, transmitter pointing errors degrade the performance of the link. Nevertheless, optimizing the shape of the transmitted beam through a metalens can improve the communication link performance. In this study, we delve into the application of metalenses for shaping laser beams in intersatellite optical communication scenarios. We present the preliminary design of the metalens and analyze its performance through numerical simulations, analyzing its feasibility and potential in space-based optical communications.

Keywords: metalens, metasurfaces, beamshaping, free space optical communications, laser communications, satellite, phase screen, phase mask

1. INTRODUCTION

Free-space optical communication (FSOC) is essential for addressing the growing demand for high-speed and secure data transmission. Unlike fiber optics, which require extensive infrastructure, FSOC offers a flexible and rapidly deployable alternative that can bridge gaps where laying fiber is impractical or too costly. Compared to radio communication, FSOC provides higher data rates, and more secure links due to its higher directivity. Inter-satellite links play a key role in establishing global FSOC networks by enabling high-speed data transfer between satellites and facilitating continuous coverage across the world. Furthermore, intersatellite links are also pivotal in supporting the future of quantum communication networks.[1]

The advantages provided by intersatellite FSOC links are offset by the challenge of managing pointing jitter in the space environment. The transmitter pointing jitter, caused by the small angular deviations of the transmitted beam, can result in significant displacement of the beam's center at the receiver's aperture plane due to the long distances involved. Traditionally, the effects of pointing jitter have been mitigated by adjusting the beam's divergence.[2] However, in a previous study,[3] the authors proposed altering not only the beam's divergence but also its far-field irradiance shape, which is typically assumed to be Gaussian. In this way, the effects of the pointing jitter are further mitigated by using the same total power of the laser source on the transmitter. Building on this concept, the current paper explores additional methods for shaping the far-field irradiance pattern, utilizing both general phase screens and metasurfaces, to enhance the resilience of FSOC links against transmitter pointing jitter and improve the overall system performance.

First in section 2, the details and models used to quantify the effect of the transmitter pointing jitter and the far-field irradiance pattern on the communication performance are presented. Then in section 3, a phase screen is proposed to shape the beam using axially symmetric Zernike polynomials. In this section, the optimization algorithms to achieve the phase screen of interest are also presented. Finally, section 4 provides a preliminary analysis of the design of a metalens for generating phase screens to shape the far-field irradiance of interest.

Further author information: (Send correspondence to M.B.A.)
M.B.A.: E-mail: m.badasaldecocea@tudelft.nl

2. POINTING JITTER AND BEAMSHAPING

Free space optical communications use a modulated laser beam to transmit information. The transmitted beam is usually considered to be Gaussian. The high directivity provided by laser beams is only exploitable to some extent, due to the pointing jitter on the transmitter side. The pointing jitter* is a stochastic process, that is mainly characterized by the pointing accuracy given by the attitude control and the coarse/fine pointing assembly (although many other factors affect the pointing jitter[4]). This pointing jitter has an impact on the performance of the system, as it deviates the peak irradiance of the transmitted Gaussian beam from the aperture of the receiver telescope. The pointing jitter is usually characterized by a probability density function (PDF) given by zero-centered Gaussian distributions in both azimuth and elevation angles.[5,6] Therefore, in the far-field and under small-angle approximation, the pointing jitter PDF is given by

$$f_{\mathrm{XY}}(x_0, y_0) = \frac{1}{2\pi\sigma^2} \exp\left(-\frac{x_0^2 + y_0^2}{2\sigma^2}\right) \tag{1}$$

where (x_0, y_0) is the location of the center of the beam in the receiver aperture plane, and $\sigma = \sigma_\theta z$ is the pointing jitter standard deviation (where σ_θ is the transmitter angular pointing jitter standard deviation in both elevation and azimuth angles). The usual residual angular pointing jitter standard deviations can range from 0.47 μrad to 22 μrad for different satellites.[7–9] This pointing jitter will create a temporal variation of the power on the receiver side, which will, in turn, affect the communication performance of the intersatellite link. The power received when the center of the irradiance field is at (x_0, y_0) can be computed by integrating the irradiance field across the aperture

$$g(x_0, y_0) = \iint_{\mathcal{A}} I(x - x_0, y - y_0)\, dxdy \tag{2}$$

where $\mathcal{A}$ is the aperture area of the receiver and $I(x, y)$ is the centered far-field irradiance. Combining the previous equations, the PDF of the received power can be computed as[10]

$$f_{\mathcal{P}}(P) = \iint_{-\infty}^{\infty} f_{\mathrm{XY}}(x_0, y_0)\ \delta\left[y - g(x_0, y_0)\right]\ dx_0\ dy_0 \tag{3}$$

Finally, this received power will determine the average bit error probability (ABEP) of the intersatellite link. For an on-off keying intensity modulation (OOK-IM), the ABEP can be computed as

$$\mathrm{ABEP} = \int_0^{\infty} \mathrm{BEP}(P)\ f_{\mathcal{P}}(P)\ dP \tag{4}$$

where $\mathrm{BEP}(P)$ is the bit error probability that is given by the Gaussian Q-function (see ref.[11]). Hence, it can be seen from the previous equations, that by changing the characteristics of the far-field irradiance pattern, the PDF of the received power and the ABEP are changed. Intuitively, the coupling between the pointing jitter and the divergence of the outgoing beam can be well understood by attending to Figure 1. In this figure, we can see that on the one hand, by increasing the beam divergence of the transmitted beam, the power fluctuations due to the transmitter pointing jitter will be lower. However, this will come at the cost of reducing the peak power that can be obtained. On the other hand, by highly collimating the beam the achievable peak power is increased but the power fluctuations increase. Previous authors tackled this issue by finding the optimum divergence of the Gaussian beam so that the ABEP is minimum.[12,13] Others followed a similar approach but optimized the outage probability instead.[14] In a previous paper, the authors proposed to also change the far-field irradiance distribution to further push the performance of the system.[3] In this paper, this beamshaping approach is further investigated, and the generation of the optimal beamshape in the far-field is done through a metalens. By shaping the wavefront of the beam, the far-field irradiance can be changed and the power can be optimally spread over the receiver aperture plane. In this way, we no longer necessarily consider a Gaussian beam[2] in the receiver aperture plane (as it is explained in the following sections). Table 1 shows the simulation parameters used for the intersatellite LEO-to-GEO link. The receiver characteristics are necessary to compute the BEP appearing in the equations above (the reader is referred to ref.[11] for more details on this model).

*the authors refer to *pointing jitter* for the full dynamic phenomena, and *pointing error* for the pointing jitter at a specific instant of time

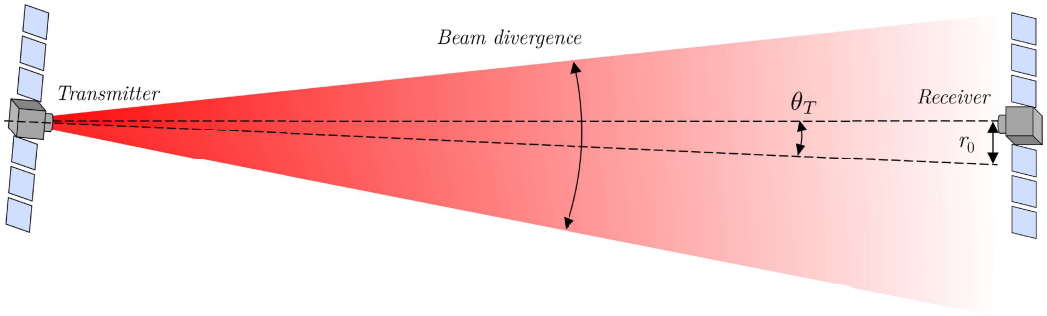

Figure 1: Effect of the transmitter pointing jitter on intersatellite free space optical communication

Description	Parameter	Value
Link distance	z	42000 km
Aperture radius	b	6.75 cm
Transmitted power	P_t	46 dBm
Receiver responsivity	R	0.8153 A/W
Receiver noise standard deviation	σ_n	4.7×10^{-9} A
Modulation	-	OOK-IM
Angular pointing jitter	σ_θ	10 μrad
Pointing jitter	$\sigma = \sigma_\theta z$	420 m

Table 1: Parameters used for the LEO-GEO link in the simulations

3. PHASE SCREEN

The first approach that we present in this paper is to use a phase screen to generate the far-field irradiance patterns of interest. In this case, the transmitter optical system is shown in Figure 2. The Gaussian beam exiting the optical fiber is first collimated by a collimating stage. Then, the collimated Gaussian beam is transmitted through a phase screen. This phase screen will shape the beam in the desired manner to give the optimum irradiance far-field of interest. To compute the desired phase screen, the following steps are followed in the simulation

1. *Fundamental Gaussian beam.* A Gaussian beam with its beamwaist located in the plane of the phase screen is created (this plane is considered $z = 0$). The field at this point is given by

$$U(x, y, 0) = U_0 \exp\left(-\frac{x^2 + y^2}{w_0^2}\right) \tag{5}$$

where w_0 is the beamwaist and the value of the electric field at the center of the beam U_0 is given as a

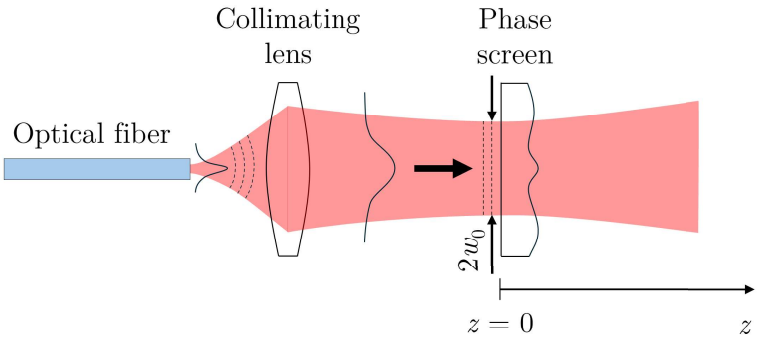

Figure 2: Simplified transmitter optical relay proposed for beamshaping in the phase screen case

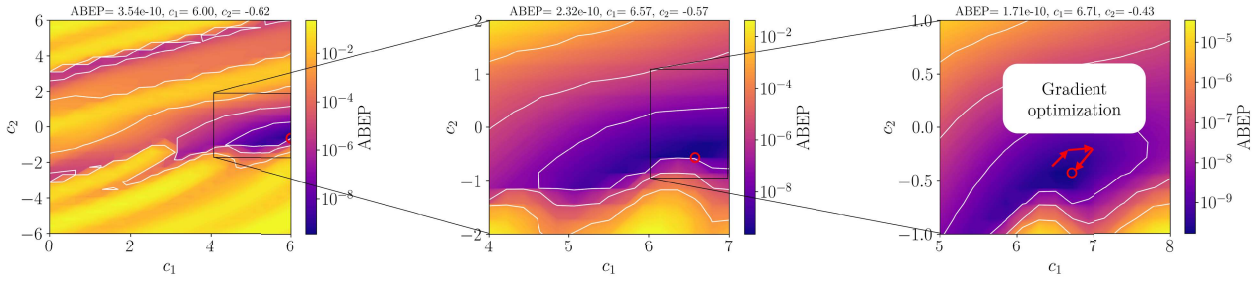

Grid search 1 Grid search 2 Grid search 3

Figure 3: Optimization procedure followed for obtaining the $\{c_1, c_2\}_{\text{opt}}$

function of the total power P_t of the beam as

$$U_0 = \sqrt{\frac{2\eta P_t}{\pi w_0^2}} \tag{6}$$

where $\eta = 377\ \Omega$ is the wave impedance on which the beam propagates (free space in this case).

2. *Generation of the phase screen.* A phase screen is applied to the Gaussian beam at $z = 0$ to shape the beam. As the incoming Gaussian beam is axially symmetric and the far-field pointing jitter PDF is also axially symmetric, the far-field irradiance solution should maintain this symmetry. Therefore, an axially symmetric phase screen is applied to the incoming Gaussian beam. Considering this, a superposition of axially symmetric Zernike polynomials Z_{2i}^0 is used to generate the phase screen of interest

$$\psi_{\text{PS}}(r) = \sum_{i=0}^{i_{\max}} c_i\ Z_{2i}^0(r) \tag{7}$$

where the c_i terms are added up to a maximum $c_{i_{\max}}$. This method of generating the phase screen is equivalent to that used in the generation of phase screen profiles for the design of diffractive optical elements.[15] The more axially symmetric coefficients c_i considered, the more degrees of freedom we have for designing the phase screen. The Zernike polynomials are defined in the unit circle, therefore the phase screen above is computed by normalizing the radial coordinate by the transmitter aperture radius $b = 6.75$ cm.

3. *Optimization of the phase screen.* The far-field irradiance pattern will vary as a function of the axial Zernike coefficients c_i. One of the possibilities when optimizing the performance of an intersatellite communication link is to minimize the ABEP. In this paper, the optimization is done with the ABEP as a function of merit. However, the work presented here is extendable to other figures of merit such as outage and fade probabilities. Furthermore, a multivariable optimization can also be performed considering several figures of merit. From all the subgroups that can be generated from the optimization variable domain $\{c_i\}_{i=1}^{i_{\max}}$ only some subsets are analyzed. To limit the design domain available the authors have chosen to investigate the following phase screen profiles given by combinations of the sets $\{c_1\}$, $\{c_1, c_2\}$, $\{c_1, c_3\}$ and $\{c_1, c_2, c_3\}$, corresponding to defocus aberration c_1, primary spherical aberration c_2 and secondary spherical aberration c_3. Several stages have been used during the optimization. Firstly, a coarse grid search has been performed to locate the surroundings of the minimum ABEP for each of the subsets above presented. After a subsequent grid search that narrows down the optimization domain, a gradient algorithm follows to locate accurately the minimum ABEP on the $\{c_i\}$ variable space domain. This optimization procedure is illustrated in Figure 3.

The previous steps have been followed to solve optimization problems given by phase screens created from three different sets of variables, i.e. $\{c_1\}$, $\{c_1, c_2\}$, $\{c_1, c_3\}$ and $\{c_1, c_2, c_3\}$. The results obtained for the minimum

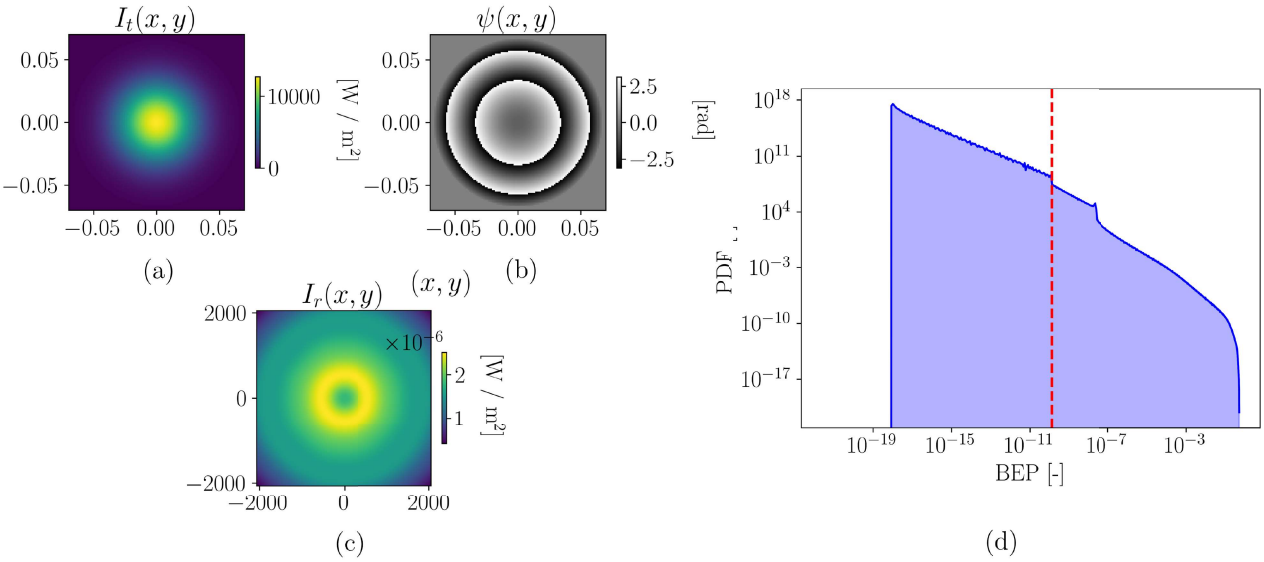

Figure 4: Optimum phase screen irradiance for the $\{c_1, c_2\}_{\text{opt}} = \{6.59, -0.48\}$ case, using the channel parameters presented in Table 1 (a) transmitted Gaussian irradiance field (b) imposed phase screen constructed with $\{c_1, c_2\}_{\text{opt}}$ (c) far-field irradiance at the receiver and (d) probability density function of the BEP created (the average ABEP is the red dashed line)

ABEP obtained through the optimization algorithm for the optimum phase screen $\{c_1, c_2\}_{\text{opt}}$ are plotted in Figure 4. Previous works have proposed to optimize the performance of the system by varying the divergence of the transmitted Gaussian beam.[2,12,16] Changing the divergence of the Gaussian beam can be interpreted physically in two different ways: changing the beamwaist w_0 of the beam (see Equation 5) or defocusing the beam ($c_1 Z_2^0$ term in Equation 7). There is a one-to-one correspondence of these two variables that will yield the same far-field irradiance pattern. However, the previous is only true as long as there is no phase wrap on the defocus phase screen affecting the beam. When the phase wraps on a phase screen with defocus the previous one-to-one correspondence does no longer hold as the phase jumps will induce diffraction patterns[15] that do not appear when only changing the beamwaist (or not wrapping the phase, as would be the case with a conventional lens). To prove the previous, Figure 5 shows the far-field irradiance patterns obtained for the beamwaist/divergence approach, and for the phase screen optimization approach. By comparing the two top left patterns, we can see that the phase wrap appearing on the defocus phase screen $\{c_1\}$ induces a diffraction pattern that is not present on the beam waist variation approach (were the field irradiance is still Gaussian). Physically the phase wrap could be avoided by having a continuous phase screen that has no phase jumps. However, when designing the metaunits constituting the metalens, this would require a continuous phase difference on a large phase range (large number of metaunits to choose from). Furthermore, it can be seen in Table 2 that the power spread due to the diffraction induced by these phase jumps is beneficial for communication performance.

In Figure 5, it can be seen that apart from defocus, a slight primary spherical aberration can further improve communication performance. The optimum far-field irradiance patterns shown in this figure extend some power beyond the $x, y \in (-2000\,\text{m}, 2000\,\text{m})$ range plotted in the figures. For the sake of emphasizing the variations of irradiance, the range is limited to the values shown in the figures. Similar results are obtained for the cases in which other sets of radial Zernike polynomials are studied. The set of optimum coefficients along with the results for the beamwaist optimization are shown in Table 2. It is shown that sequentially adding a higher order of Zernike polynomials yields a lower ABEP. The power spread induced by the proposed phase screens is therefore beneficial in terms of ABEP.

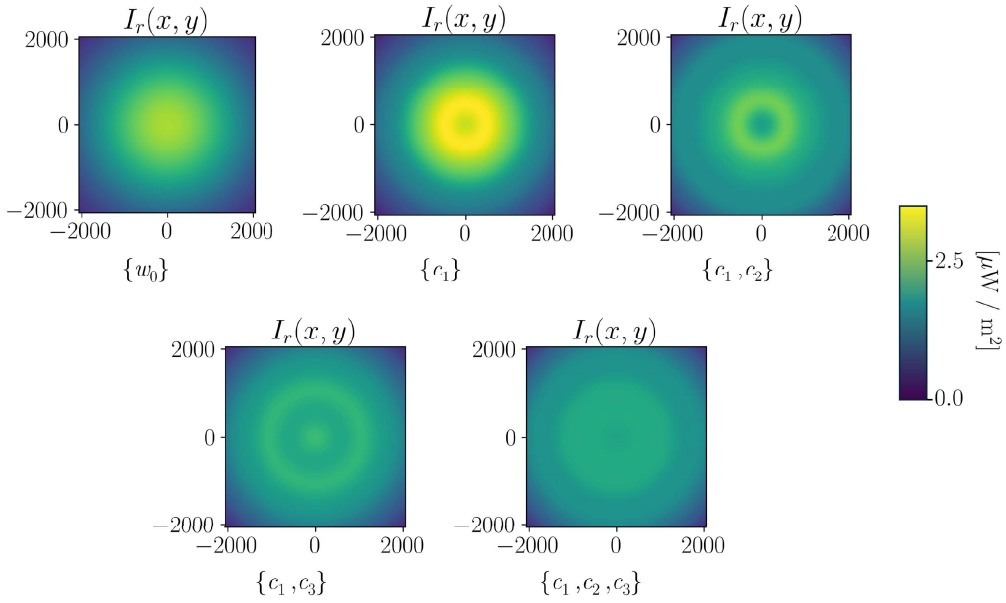

Figure 5: Optimum far-field patterns on the receiver aperture plane obtained for the phase screens shown in Table 2

Set of $\{c_i\}$	**Optimum values**	$\log_{10}$ (ABEP)
$\{c_1\}$	$\{6.73\}$	-8.75
$\{c_1, c_2\}$	$\{6.59, -0.48\}$	-9.88
$\{c_1, c_3\}$	$\{7.07, 0.29\}$	-9.71
$\{c_1, c_2, c_3\}$	$\{6.81, -0.33, 0.18\}$	-10.08
Beamwaist/divergence approach		
$\{w_0\}$	$\{6.87$ mm$\}$	-8.56

Table 2: Results obtained for the optimization of the phase screens and the beamwaist/divergence approach

4. METALENS DESIGN

In the previous section, the beamshaping was performed through a phase screen for which the characteristic length of the phase variation could be done over orders of magnitude above the wavelength of the electromagnetic field. These phase screens could be realized physically through diffractive optical elements or free-form optics. Mathematically, the scale condition mentioned can be written as

$$\max(\psi(\mathbf{r}) - \psi(\mathbf{r} \pm \lambda)) \lll \mathcal{O} \tag{8}$$

. By contrast, metasurfaces are based upon the construction of patterns of nanostructures that impinge phase, polarization, and amplitude changes of the field at the subwavelength scale.[17] Metamaterials and metasurfaces hold significant promise for space applications due to their compactness and lightweight characteristics. These devices use nanostructures embedded in their flat surfaces to manipulate the electromagnetic field for various purposes. Prior research has already highlighted the benefits of employing metalenses, including enhanced detection efficiency amidst receiver angle of arrival jitter and improved coupling to fiber efficiency in duplex free space optical communication terminals.[18,19] By tuning the geometries and materials of the metaunits the scattering properties of these can be changed, yielding a huge flexibility of the output electromagnetic field properties. In this section, we present the preliminary design of a metalens built to shape the far-field irradiance pattern on an intersatellite link. Firstly, we present the analysis of the metaunits forming the metalens.

4.1 Metaunit design

A metaunit is the fundamental building block of a metamaterial, engineered to manipulate electromagnetic waves. It works by scattering incoming waves through its subwavelength structure, altering the properties of the electromagnetic field. There are several techniques that can be used to simulate the metaunit: Finite Element Method (FEM), Finite Difference Time Domain (FDTD) or Rigurous Wave Coupled Analysis (RCWA), being the most used. In this paper, we present the result obtained through FEM in the frequency domain using COMSOL Multiphysics.[20] The design and analysis of metasurfaces are usually performed following two simulation steps.[21] First of all, the metaunit is simulated under local uniformity approximation. This last approximation involves simulating the metaunit under periodic boundary conditions. Physically, these results are only valid on an infinite array of equal geometry metaunits. However, this is a good first-order approximation to design the metalens (although the coupling effects between non-equal metaunits have to be considered for a more accurate computational result). The second step is designing the whole metasurface (based on the results obtained for each metaunit) and simulating it. In this subsection, the first step is covered. Other design approaches involve designing all the metunits at once, considering from the beginning the coupling between different geometry shapes on the nanoantennas.[22]

Following previous works done in metalenses for the 1550 nm wavelength, widely used in optical communication applications, the following physical properties have been assigned to the metaunit.[18,19] The substrate of the metaunit is made of silica (SiO_2). The cylindrical nanopillars are made of silicon (Si) and have a height $H = 1000$ nm. The parameter varied to obtain the different phase shifts of interest is the diameter D of the nanopillar which ranges from 100 to 350 nm. The period of the metunit is set to $L = 400$ nm. The results obtained in the simulation are shown in Figure 6.

By using a cylindrical nanopillar of high refractive index and varying the diameter of this, a full 2π phase range can be obtained for the outgoing electromagnetic wave as is shown in Figure 6(c). The transmission efficiency of the nanopillars as a function of the diameter is also shown in the same figure, where it can be seen that low efficiencies appear when the diameter approaches the size of the lattice period. The resonances appearing on the nanopillars of the metaunit can be seen in the magnetic fields illustrated in Figure 6(b).

4.2 Metalens design considerations

From the response of the nanopillars obtained in Figure 6, a first iteration of the resulting metalens can be done. Discretizing the diameters on the continuous shown in Figure 6 we can create a discrete set of available phase delays. At this point, there are two approaches to designing the metalens

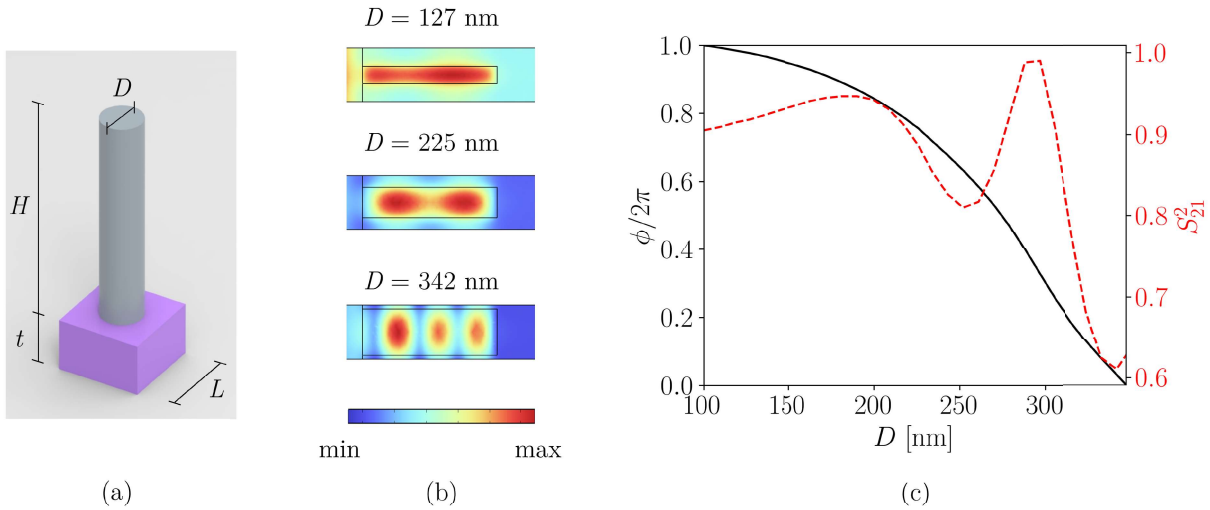

(a) (b) (c)

Figure 6: Design of the metaunit. (a) illustration of the cylindrical nanopillar and the dimensions involved, (b) normalized magnetic field norm for different nanopillar diameter sizes, and (c) normalized phase and transmission of the nanopillars for different diameter sizes

- The first approach consists of generating exactly the same phase screen as the one obtained in the previous section. This would mean replacing the phase screen in Figure 2 by a metalens. Therefore, this would imply building a large area metalens.[23] The benefit of this approach is that, given the small size of the nanopillars a very high resolution of the ideal phase screen could be achieved. However, the disadvantage is that simulating a large area of metalens is computationally very expensive,[23] and does not provide a great space saving compared to more conventional bulk optical elements.

- The second approach would be to design a smaller phase screen where the beamwaist w_0 of the Gaussian beam involved would be on the order of tens of microns. This would mean that we would use a total of $\sim 10^4 - 10^6$ nanopillars to design this phase screen. Although the resolution of the phase screen could be smaller, it might still be sufficient for generating the far-field irradiance shapes of interest.

A detailed numerical analysis of the resulting metalens design would require simulating the whole metalens with one of the electromagnetic computational methods above mentioned, i.e. FEM, RCWA, FDTD. This is because the periodicity conditions that have been used to simulate the metaunits are no longer applicable as the resulting metalens has its metaunits surrounded by different geometries in an asymmetric manner. However, as a first-order approximation of the resulting field to assess the feasibility of building a phase screen with a metalens built upon the metaunits presented in subsection 4.1, the whole metalens is simulated by simulating not only a phase screen (as in section 3) but adding a transmission screen that is given by the respective S_{21}^2 for each of the pixels of the phase screen. This gives the first approximation of how much the metalens can approximate to the ideal phase screen, and how much these discrepancies affect the communication performance of the system. The results of the simulation are shown in Figure 7 for the set of coefficients $\{c_1, c_2, c_3\}$. The resulting communication performance parameter is $\log_{10}(\text{ABEP}) = -7.72$, which is orders of magnitude worse than the achieved with the ideal phase screen, where $\log_{10}(\text{ABEP}) = -10.08$ (see Table 2). It is the authors' opinion that the low transmission efficiency of the nanopillars (especially in the large diameter range shown in Figure 6(c)), is very detrimental and the improvement due to the redistribution of the power in the far-field induced by the metalens is still not enough to compensate for the power losses due to the transmission efficiency of the nanopillars. Therefore, further research is required to improve the design of the nanopillars by increasing their transmission efficiency so that they can be used to shape the laser beams of interest.

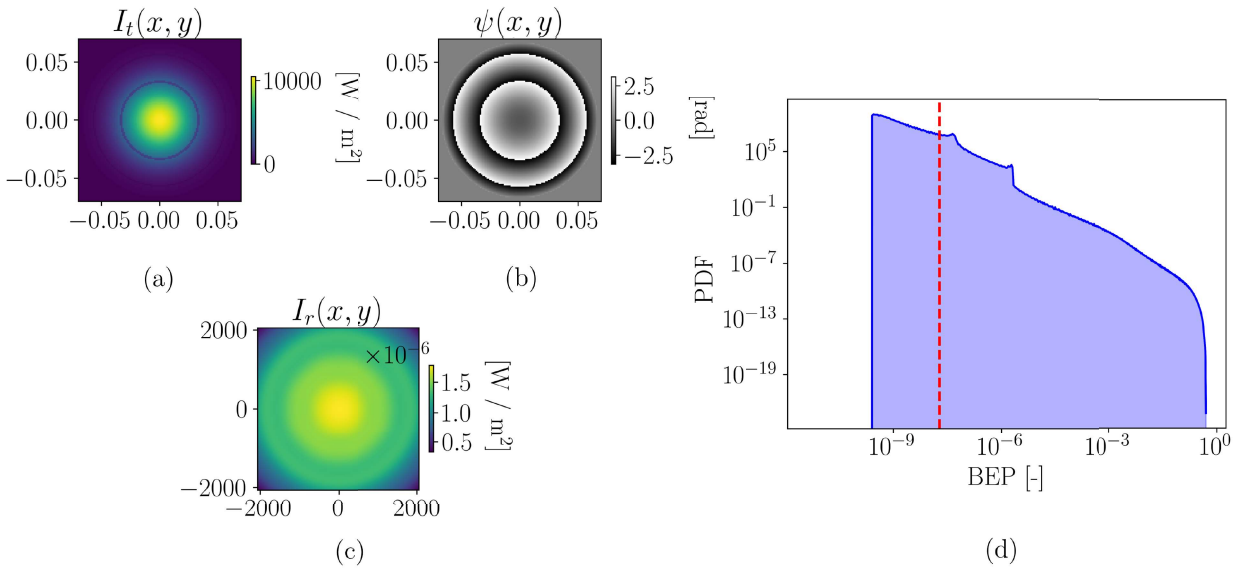

Figure 7: Results of the field obtained for the simplified simulation of the metalens, (a) shows the the transmitted irradiance field affected by the transmittance of the nanopillars (b) shows the phase screen fo the transmitted beam (c) is the far-field irradiance pattern generated and (d) is the PDF of the BEP

5. CONCLUSIONS AND FUTURE WORK

In this paper, it has been demonstrated that by altering the far-field irradiance pattern, the performance of intersatellite FSOC links can be significantly improved. To generate physically feasible far-field patterns, a phase screen was proposed to reshape the original Gaussian beam. This phase screen was created using axially symmetric Zernike polynomials, with an optimization algorithm employed to identify the locally optimal phase screens for mitigating the effects of pointing jitter. Finally, a preliminary design of a metalens capable of acting as a phase screen was presented, with simulations of metaunits that provide a full 2π phase shift, showcasing the potential for practical implementation in enhancing FSOC systems.

Future work will focus on exploring the potential for increased performance by incorporating higher-order axially symmetric Zernike polynomials in the design of the phase screens. This approach could offer further improvements in mitigating pointing jitter in intersatellite FSOC links. However, to a first-order approximation, creating the optimum phase screens through a metalens built upon the proposed nanopillars is not better than the conventional approach of optimizing the divergence of a Gaussian beam. The benefits of shaping the transmitted beam by using the proposed nanopillars do not compensate for the transmission losses when the light goes through these devices. Therefore, higher efficiency nanopillars are needed in the whole phase range for a metalens to be efficient enough for its use in beamshaping for intersatellite optical communications. This could be achieved by considering other nanopillar shapes and/or varying both the height and diameter of the cylindrical nanopillars presented in this work. Furthermore, asymmetrical nanopillar schemes providing bound states in continuous could also improve the transmission efficiency at a specific wavelength.[17] The design of the metalens using the proposed metaunits is also under investigation by the authors, where its size is a decisive factor that can affect both the design of the overall transmission optical relay and the computational analysis feasibility of the metalens.

ACKNOWLEDGMENTS

The authors would like to thank the support from the Dutch Research Council (NWO) for funding the Perspectief Project P19-13 "Optical Wireless Super Highways".

REFERENCES

[1] Liao, S.-K., Yong, H.-L., Liu, C., Shentu, G.-L., Li, D.-D., Lin, J., Dai, H., Zhao, S.-Q., Li, B., Guan, J.-Y., Chen, W., Gong, Y.-H., Li, Y., Lin, Z.-H., Pan, G.-S., Pelc, J. S., Fejer, M. M., Zhang, W.-Z., Liu, W.-Y., Yin, J., Ren, J.-G., Wang, X.-B., Zhang, Q., Peng, C.-Z., and Pan, J.-W., "Long-distance free-space quantum key distribution in daylight towards inter-satellite communication," *Nature Photonics* **11**, 509–513 (Aug. 2017).

[2] Toyoshima, M., Jono, T., Nakagawa, K., and Yamamoto, A., "Optimum divergence angle of a Gaussian beam wave in the presence of random jitter in free-space laser communication systems," *JOSA A* **19**, 567–571 (Mar. 2002).

[3] Badás, M., Piron, P., Bouwmeester, J., and Loicq, J., "On the optimum far-field irradiance distribution using Laguerre-Gaussian beams for intersatellite free-space optical communications," *Optics Express* **32**, 31597–31620 (Aug. 2024).

[4] Badás, M., Piron, P., Bouwmeester, J., Loicq, J., Kuiper, H., and Gill, E., "Opto-thermo-mechanical phenomena in satellite free-space optical communications: survey and challenges," *Optical Engineering* **63**, 041206 (Oct. 2023).

[5] Toyoshima, M., Takayama, Y., Kunimori, H., Jono, T., and Yamakawa, S., "In-orbit measurements of spacecraft microvibrations for satellite laser communication links," *Optical Engineering* **49**, 083604 (Aug. 2010).

[6] Wang, X., Wang, X., Li, C., Jia, J., Jia, J., Wu, J., Shu, R., Shu, R., Zhang, L., Zhang, L., Zhang, L., Wang, J., Wang, J., Wang, J., and Wang, J., "Angular micro-vibration of the Micius satellite measured by an optical sensor and the method for its suppression," *Applied Optics* **60**, 1881–1887 (Mar. 2021).

[7] Chen, Y.-L., Ma, J., Tan, L., and Wang, Q., "Angular dispersion analysis of DOE-WDM," in [*Holography, Diffractive Optics, and Applications II*], **5636**, 409–416, SPIE (Feb. 2005).

[8] Chang, J., Schieler, C. M., Riesing, K. M., Burnside, J. W., Aquino, K., and Robinson, B. S., "Body pointing, acquisition and tracking for small satellite laser communication," in [*Free-Space Laser Communications XXXI*], **10910**, 144–152, SPIE (Mar. 2019).

[9] Cahoy, K., Grenfell, P., Crews, A., Long, M., Serra, P., Nguyen, A., Fitzgerald, R., Haughwout, C., Diez, R., Aguilar, A., Conklin, J., Payne, C., Kusters, J., Sackier, C., LaRocca, M., and Yenchesky, L., "The CubeSat Laser Infrared CrosslinK Mission (CLICK)," in [*International Conference on Space Optics — ICSO 2018*], Karafolas, N., Sodnik, Z., and Cugny, B., eds., 33, SPIE, Chania, Greece (July 2019).

[10] Thomas, J. B., [*Introduction to Probability*], Springer (1986).

[11] Badás, M., Bouwmeester, J., Piron, P., and Loicq, J., "Impact of transmitter wavefront errors and pointing jitter on intersatellite free space optical communications," in [*Computational Optics 2024*], **13023**, 1302302, SPIE (June 2024).

[12] Do, P. X., Carrasco-Casado, A., Vu, T. V., Hosonuma, T., Toyoshima, M., and Nakasuka, S., "Numerical and analytical approaches to dynamic beam waist optimization for LEO-to-GEO laser communication," *OSA Continuum* **3**, 3508–3522 (Dec. 2020).

[13] Toyoshima, M. and Araki, K., "In-orbit measurements of short term attitude and vibrational environment on the Engineering Test Satellite VI using laser communication equipment," *Optical Engineering* **40**, 827–832 (May 2001).

[14] Farid, A. A. and Hranilovic, S., "Outage Capacity Optimization for Free-Space Optical Links With Pointing Errors," *Journal of Lightwave Technology* **25**, 1702–1710 (July 2007).

[15] Wood, A. and Babington, D. J., [*Diffractive Lens Design: Theory, design, methodologies and applications*], Institute of Physics Publishing (Aug. 2022).

[16] Carrasco-Casado, A., Shiratama, K., Kolev, D., Trinh, P., Fuse, T., Fuse, S., Kawaguchi, K., Hashimoto, Y., Hyodo, M., Sakamoto, T., Kunisada, T., and Toyoshima, M., "Prototype Development and Validation of a Beam-Divergence Control System for Free-Space Laser Communications," *Frontiers in Physics* **10** (May 2022).

[17] Brener, I., Liu, S., Staude, I., Valentine, J., and Holloway, C., eds., [*Dielectric metamaterials*], Elsevier (2020).

[18] He, N., Guo, T., Tian, J., Du, J., Hu, Z., Xing, Y., Jin, Y., Zhang, J., and He, S., "High-Speed Duplex Free Space Optical Communication System Assisted by a Wide-Field-of-View Metalens," *ACS Photonics* **10**, 3052–3059 (Sept. 2023).

[19] Islam, M. S., Shahverdi, K., and Boyraz, O., "Metalens integrated receiver to reduce the effect of angle of arrival jitter in free space optical communication," *JOSA B* **40**, 891–899 (Apr. 2023).

[20] COMSOL AB, "COMSOL Multiphysics®."

[21] So, S., Mun, J., Park, J., and Rho, J., "Revisiting the Design Strategies for Metasurfaces: Fundamental Physics, Optimization, and Beyond," *Advanced Materials* **35**(43), 2206399 (2023).

[22] Ji, W., Chang, J., Xu, H.-X., Gao, J. R., Gröblacher, S., Urbach, H. P., and Adam, A. J. L., "Recent advances in metasurface design and quantum optics applications with machine learning, physics-informed neural networks, and topology optimization methods," *Light: Science & Applications* **12**, 169 (July 2023). Number: 1 Publisher: Nature Publishing Group.

[23] She, A., Zhang, S., Shian, S., Clarke, D. R., and Capasso, F., "Large area metalenses: design, characterization, and mass manufacturing," *Optics Express* **26**, 1573 (Jan. 2018).